PLASMA PARTICLE TRAJECTORIES AROUND SPACECRAFT PROPELLED BY ION THRUSTERS

H. B. Liemohn, R. L. Copeland, and W. M. Leavens
Boeing Aerospace Company

ABSTRACT

Ion thrusters are being considered for propulsion of future spacecraft due to their relatively low fuel mass to thrust ratio and easy access to solar power for long duration missions. Operation of such thrusters requires high spacecraft potentials, and their local electric fields can draw return current from the thruster plasmas, reducing system efficiency. In this paper, the thruster plasma is assumed to be described by a collimated energetic beam (∿10 keV) and a cloud of ionized thermal propellant (∿10 eV) produced by charge-exchange. A simple adiabatic model is used to describe the expansion of these neutral plasmas away from the source. As the pressure falls, shielding currents dissipate, and the geomagnetic field takes control of the particles. In low earth orbit, it is concluded that the vehicle easily outruns its thruster plasma. At geosynchronous altitude, the local electric fields around high voltage surfaces collect return current from the thermal plasma that appears to be limited only by the available space charge. Results appropriate to proposed electric propulsion missions and the solar power satellite are presented and operational considerations are discussed.

INTRODUCTION

Spacecraft requirements for long-duration missions and minimum vehicle weight have enhanced interest in ion thrusters that operate from solar energy. Although these propulsion systems have low thrust, their low mass to overall thrust during prolonged missions makes them strong candidates for interplanetary explorations to comets and asteroids and as a means of station keeping for geosynchronous payloads. They are also attractive for orbit-transfer propulsion when time is not a primary limitation.

A number of small thrusters have been built and tested in space and the laboratory (e.g., refs. 1-4). Somewhat larger propulsion modules have been conceived for future large-scale applications (refs. 5,6). All of these thrusters generate a thermal plasma in a chamber and accelerate the ions across closely spaced grids. The high grid voltage collimates the ion beam, and an adjacent electron source provides immediate neutralization. A secondary source of plasma at the outlet occurs by charge exchange between the beam ions and escaping neutral atoms. Approximately 15% of the beam charge is transferred to these thermals which represent a significant source of local current. Some operational characteristics of these thrusters are summarized in table I.

TABLE I. NOMINAL ION THRUSTER CHARACTERISTICS
(refs. 5-7 and D. Grim, private communication)

Source Grid Diameter (cm)	30	100
Propellant Gas	Hg	A
Beam Current (A)	2	80
Acceleration Voltage (kV)	1.1	10*
Exit Plane Beam Density (ions/cm^3)	$\sim 5 \times 10^9$	
Exit Plane Thermal Density (ions/cm^3)	$\sim 10^{11}$	
Thermal Ion Current (A)	0.2	~8
Efficiency (%)	70	80
Thrust (N)	0.13	6

*Solar power satellite station keeping operation at geosynchronous altitude.

The plasma environs around the spacecraft consist of both thruster exhaust and natural background. Some characteristics of these plasmas that are needed in the following analysis are presented in table II. Only operations in low earth orbit (LEO) around 400 km altitude and geosynchronous earth orbit (GEO) at 6.6 earth radii geocentric are considered here to demonstrate the effects. The spacecraft is assumed to be following a circular trajectory so that its speed relative to the background magnetoplasma is 7.7 km/sec at LEO and nearly zero at GEO. At LEO the natural plasma density is adequate to shield the spacecraft fields from the thruster plasma. However, the tenuous conditions at GEO allow fields to extend well beyond the vehicle dimensions.

TABLE II. PLASMA ENVIRONMENT PARAMETERS
(refs. 7-8)

		LEO at 400 km	GEO at 36,000 km	
		Natural Plasma	Argon Thruster Plasma	
			Beam	Thermal
Ion Density (m^{-3})	LEO	$10^6 - 10^7$	-	-
	GEO	$10^{11} - 10^{12}$	-	-
Ion Thermal Energy (eV)	LEO	0.1	10	10
	GEO	1 - 10		
Ion Mean Free Path (km)	LEO	~10	$\sim 10^2$	10
	GEO	$\sim 10^6$	$\sim 10^7$	10^3
Ion Larmor Radii (km)	LEO	1	2	0.5
	GEO	1,000	500	60
Debye Length (cm)	LEO	~0.8	0.03 (at exit plane)	0.007
	GEO	~800		

For ion propulsion to operate efficiently from solar energy, a high voltage solar array is required to avoid the extra weight of power converters. The local electric fields around these panels can attract the thruster plasma if Debye shielding by the ambient plasma is inadequate. Additionally, as the thruster plasma disperses, the geomagnetic field eventually takes control of the particles, and some geometries permit orbits to fold back on the vehicle surface. Such return current diminishes the effectiveness of the overall system by inhibiting propulsion and/or leaking power from the solar energy collectors.

The purpose of this paper is to investigate the interaction of the thruster plasma with its parent power source. The intention is to understand the plasma behavior qualitatively and make quantitative assessments where return current may be significant. The goal is to identify modes where there are negligible system losses, determine characteristics of modes where return current levels impact the system efficiency, and explore ways to modify inefficient configurations. In the following section a model is developed for the expansion characteristics of the energetic beam and thermal plasma. The next section describes the role of the geomagnetic field. The spacecraft field effects are treated in the last section.

THRUSTER PLASMA EXPANSION

Rather than solve the nonlinear MHD fluid equations numerically for equilibrium conditions, a less complicated approach is presented in which the trajectory equation for the average plasma column radius with time is derived analytically from conservation of energy and adiabatic constraint equations. The adiabatic fluid equations are used because they are often a valid approximation for collisionless systems. The only requirement is that the third moment of the distribution function around the mean expansion speed must be small. This, along with conservation of particles, yields an equation for the average plasma density with time. It is solved only for the ion motion, assuming that there exists a charge neutralizing background of electrons that follow the ions.

From conservation of energy,

$$1/2\ M\ \bar{v}^2 = k(T_o - T) \tag{1}$$

where M is the ion mass, v is the local mean ion velocity, k is Boltzmann's constant, T_o is the thermal ion temperature at the source, and T is the local ion temperature along the beam. The adiabatic constraint equation is

$$T/N_\ell^{\gamma-1} = T_o/N_o^{\gamma-1} \tag{2}$$

where N_ℓ is the line plasma density, N_o is the source density, and γ is the ratio of specific heats which has the value 5/3 here.

Since the divergence angle of ion trajectories exiting the accelerating diode is small, and the axial ion speed greatly exceeds the rocket speed, a line source plasma model with radial adiabatic expansion can approximate the beam plasma expansion. Assuming no end losses, conservation of particles requires

$$N_\ell/N_o = (r_o/r)^2 \tag{3}$$

where r_o and r are the column radii at the thruster and along the beam. Integrating the differential equation resulting from eqs. (1), (2), and (3), gives an implicit expression for r(t),

$$\bar{v}_o\, t = \left(\frac{3}{4}\right) r_o \left[\left(\frac{r}{r_o}\right)^{2/3} \left[\left(\frac{r}{r_o}\right)^{4/3}-1\right]^{1/2} + \log\left[\left(\frac{r}{r_o}\right)^{2/3} + \left(\frac{r}{r_o}\right)^{4/3}-1\right)^{1/2}\right]\right] \tag{4}$$

where $\bar{v}_o$ is the initial plasma thermal velocity. Equation (4) may be solved numerically. From eqs. (1) to (3) one can easily obtain $N_\ell(t)$, $T(t)$, $\bar{v}(t)$, and $z = ut$, where u is the directed beam speed.

A Gaussian angular distribution is assumed to account for beam divergence at the source. Combining these results leads to an expression for the beam envelope,

$$N(\theta,z) = N_\ell(z)\; e^{-|\theta/\theta_o|^2} \tag{5}$$

where N_ℓ is the axial density calculated as above, θ is the angle with respect to the z axis, and θ_o is typically 3°. Figure 1 shows beam plasma density contours for a one meter argon 100 cm thruster at two different times

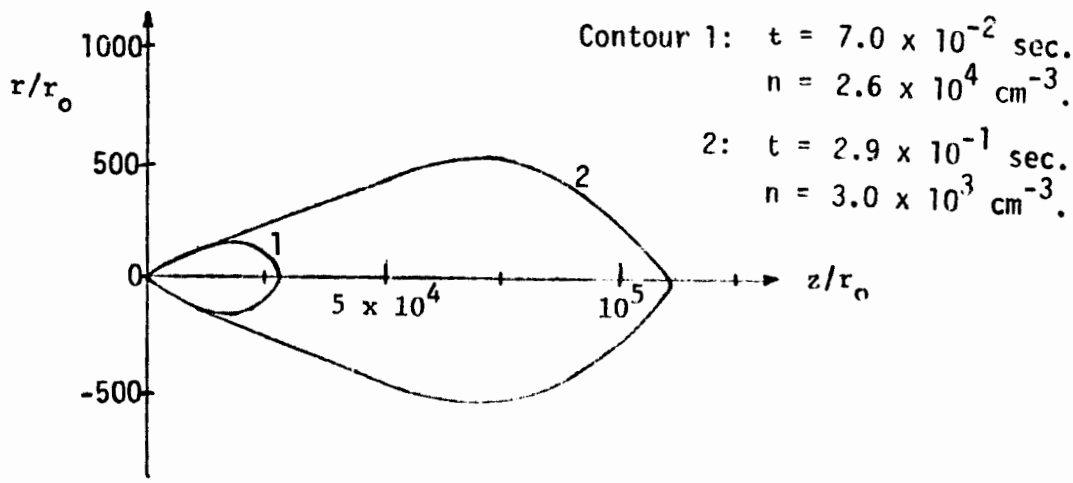

Figure 1. - Beam plasma density contours for argon SPS thruster.

Thermal Plasma

Charge transfer within the beam, between the slow neutrals and the fast ions, produces a relatively high density cool plasma which remains in the neighborhood of the thruster. The source characteristics of this plasma plume depend upon the charge transfer production rate and the subsequent motion of the slow ions which are described in the Appendix. The latter step is considerably more complicated, because the ion dynamics are dominated by the electrostatic potential structure in the charge transfer region, which in turn is determined by the beam neutralization process.

Here, the adiabatic model is assumed to adequately describe the motion of the thermal plasma away from the source. However, the isotropic motion of neutrals suggests hemispherical expansion so that conservation of particles now has the form

$$n_s/n_o = (r_o/\rho)^3 \tag{6}$$

where n is density and ρ is radial distance. Following the same analysis as before, yields an explicit equation for $\rho(t)$,

$$\frac{\rho}{r_o} = \left[1 + \left(\frac{v_o t}{r_o}\right)^2\right]^{1/2} \tag{7}$$

where $\bar{v}_o$ is the mean velocity in the source region. Similarly, expressions for $n_s(t)$, $T(t)$, and $\bar{v}(t)$ may be obtained. The initial density distribution of neutrals is assumed to have a cos θ angular distribution (ref. 7). Consequently, the thermal density envelope has the form

$$n(\theta,\rho) = n_s(\rho) \cos\theta \tag{8}$$

Figure 2 shows density contours of the thermal plasma from the argon thruster for two different times. Note that the density levels for the contours in both figures 1 and 2 are the same. Also, it is important to note that the beam plasma escapes the spacecraft region easily while the slower thermal plasma remains in the vicinity of the spacecraft.

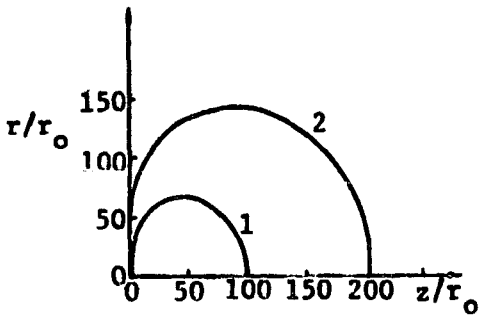

Contour 1: $t = 8.7 \times 10^{-3}$ sec, $n = 2.6 \times 10^{4}$ cm^{-3}

2: $t = 1.7 \times 10^{-2}$ sec, $n = 3 \times 10^{3}$ cm^{-3}

Figure 2. - Thermal plasma density contours for argon SPS thruster.

GEOMAGNETIC FIELD EFFECTS

The thruster plasma is sufficiently dense in the vicinity of its exit plane. (see table I) to generate its own currents that buck out the geomagnetic field. As the beam and thermal plasmas expand however, these currents are dispersed, and the geomagnetic field eventually takes control of the individual particles. An exact treatment of this transition process is extremely complex and beyond the scope of this paper. A simple pressure balance criterion is used instead, since the exact transition process does not appear to affect the conclusions. The motion of the particles is described by conventional adiabatic theory (e.g., refs. 10, 11) ac the local geomagnetic field is fairly uniform locally. The effect of spacecraft electric fields is treated in the next section.

Due to the large ion Larmor radii and mean free paths compared to characteristic plasma dimensions (see table II), a continuous transition from the plasma fluid to single particle orbits probably extends over an appreciable fraction of the thermal and beam plasma plumes. The pressure balance expression

$$\frac{1}{2} NM \bar{v}^2 = B^2/8\pi \qquad (9)$$

where B is the geomagnetic field, is recognized as a gross approximation. However, it serves a useful purpose as the estimated locations of the transitions are found to be relatively close to the source. Injection velocities for ions into the geomagnetic field are assumed to be those of the free expansion, since the Larmor radii are large. These assumptions provide a reasonably consistent model for estimating geomagnetic effects.

Beam Plasma

From the beam qualities described by eq. (5) and displayed in fig. 1, it is evident that these energetic ions are well collimated. Substituting these density envelopes into eq. (9) and evaluating at LEO and GEO gives the transition values shown in table III. Comparison of these results with those in table II confirms the assumption regarding the lack of geomagnetic distortion through the transition.

TABLE III. THRUSTER PLASMA FLUID TO PARTICLE ORBIT TRANSITION LOCATION

	B (gauss)	Density N or n_3 (ions/cm^3)	Beam z/r_o	Beam r/r_o	Thermal ρ/r_o
LEO (400 km)	0.31	2.4×10^8	63	2.9	4.8
GEO (36,000 km)	0.0011	2.9×10^3	40,000	400	208

The ion-beam directed velocity is substantially greater than that of the spacecraft at LEO as well as at GEO. Consequently, these ions enter the geomagnetic field with their beam speed. Since their thermal motion is small as well, their pitch angle relative to the geomagnetic field is nearly equal to the angle between the thruster direction and the field. These ions follow well known first-order adiabatic orbits along geomagnetic flux tubes (e.g., refs. 10, 11). Depending on their mirror altitude, they may be trapped for an extended period (possibly years above LEO).

Most applications at LEO involve accelerating spacecraft to attain higher altitude and the ion beam is directed at a large angle to the field. The tilt of the geomagnetic axis relative to the earth's axis and appreciable trajectory inclinations can produce angles as small as 30° or less, however. If the beam is directed toward the atmosphere, the particles are completely absorbed in the spacecraft hemisphere; if the beam is directed upward it travels to the opposite hemisphere, where it is deposited.

At GEO the spacecraft is usually stationary in the geomagnetic field, and the ion beam may be directed at any angle with respect to the field depending upon its purpose. Generally the beam ions are injected into trapped orbits of long duration. Their longitudinal drift motion and subsequent dispersion is expected to eliminate any appreciable return current to the spacecraft. However, some caution is advised to avoid those rare conditions around the geomagnetic equator that create particle mirror locations close to the vehicle which could cause bursts of return current. At the opposite extreme, beams injected nearly parallel to the field (within the loss cone) follow the flux tube down to the atmosphere where they are absorbed. Due to the variety of possible operating conditions, no attempt is made to provide quantitative results here, although they are readily calculable.

Thermal Plasma

Due to its hemispherical expansion, the thermal plasma density falls much faster than that of the beam. Consequently, its transition location is very close to the vehicle as indicated by the values in table III. Furthermore, the thermal plasma does not function as independently of the spacecraft as the beam can; the plume stays close to the vehicle until the field takes control. Thus, these ions cause concern as a possible return current source.

The motion of the thermal ions is most easily perceived in the rest frame of the spacecraft as a continuum of expanding spheres, which is depicted schematically in figure 3. As the plume density drops to the transition threshold defined by eq. (9), the rearward hemisphere acts as a source surface for injection into the geomagnetic field. Alternatively, in the laboratory frame the ion motion is perceived as a vector sum of the spacecraft velocity and radial expansion vector as shown in figure 4. This vector diagram is valid for all times of interest since the expansion motion is radial at nearly constant speed and the Larmor radii are large compared with the plume dimensions (table II). At the outer boundary the mean thermal expansion is 6.9 km/sec compared to the spacecraft speed of 7.7 km/sec at LEO.

At LEO it is evident from figure 4 that the plume cannot "catch up" to the spacecraft (when local electric fields are omitted from consideration), because thermal speed is directed into the hemisphere away from the vehicle. Even those ions in the energetic Maxwellian tail of the thermal plasma move away due to lack of collisions back toward the vehicle. A typical cluster of thermal ion orbits is shown in figure 5 for the case where the spacecraft is being propelled normal to the local geomagnetic field.

The thermal ions emanating from a geosynchronous satellite thruster would follow geomagnetic orbits like those in figure 5 assuming no electric fields were present; however, the scale is now 300 times larger (see Larmor radii in table II). Those ions injected nearly orthogonal to the local geomagnetic field can return to the spacecraft after one gyration if their velocity components satisfy the inequality

$$v_{\parallel}/v < \ell_{\parallel}\,(\mathrm{km})/60\pi \qquad (10)$$

where $v_{\parallel}$ is the velocity component parallel to the field, v is total ion speed, and $\ell_{\parallel}$ is the dimension of the spacecraft parallel to the field. For a typical 100 m extension less than 0.0005 of the thermal ion charge would be collected directly; the rest enter trapped orbits.

All the other ions travel away along geomagnetic flux tubes until they mirror and return past the plane of the spacecraft. From adiabatic theory for geomagnetically trapped particles (e.g., refs. 10, 11), the time to return to the spacecraft is on the order of $2\,R_e/\bar{v}$, where R_e is the geocentric distance to the spacecraft. For argon ions at 10 eV, this bounce time is $\sim 1.2 \times 10^4$ secs. During this time they drift in longitude at the rate of about 3×10^{-8} rad/sec, which corresponds to an equatorial transit distance of 1500 km, well away from the spacecraft.

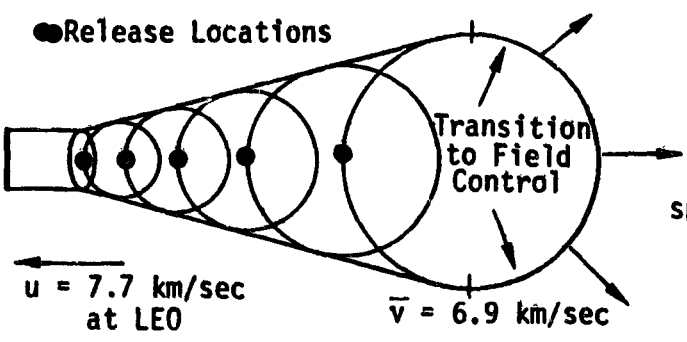

Figure 3. - Thermal ion plume expansion (spacecraft frame).

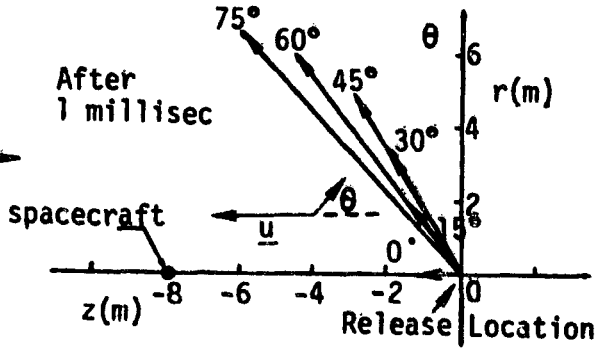

Figure 4. - Thermal ion trajectories at LEO (laboratory frame).

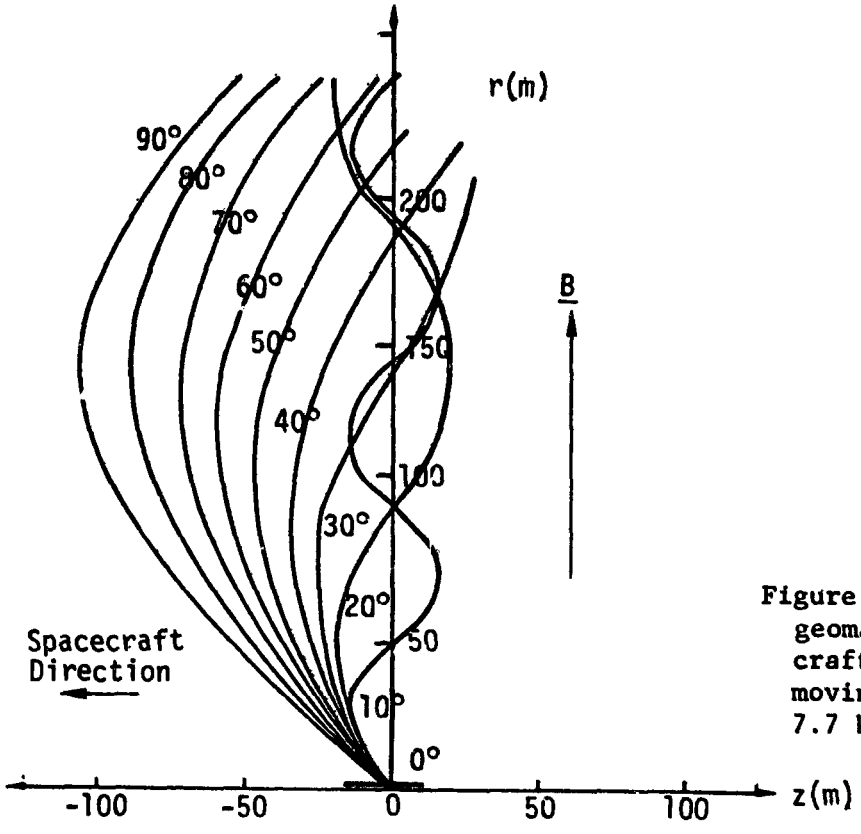

Figure 5. - Thermal ion geomagnetic orbits (spacecraft thruster at LEO moving across $\underline{B}$ at 7.7 km/sec).

SPACECRAFT FIELD EFFECTS

Spacecraft that employ ion thrusters for propulsion will probably use solar arrays to generate their electrical power. Since significant propulsion can only be achieved with high power levels, the array will undoubtedly operate at high voltages to reduce conduction losses. Such potentials on exterior spacecraft surfaces produce regions of high electric field which can dramatically alter the thruster plasma. Since the thermal plasma cloud lingers in the vicinity of the spacecraft, the ions and electrons are easily attracted back to the vehicle by these fields. If the surface is insulated, space charge can build up to neutralize the applied fields. If there is access to non-insulated conductors, as, for example, exposed solar cell connectors, the return current shortcircuits the system, lowering efficiency. Presumably the main thruster beam operates at such an energy and distance from these field sources that it remains unaffected.

A spacecraft driven internally to high voltages behaves like a floating double probe (refs. 12, 13). Its potential distribution is biased negative due to the higher mobility of electrons. Experience has shown that a double probe in an ionospheric plasma with an impressed voltage V has its positive end at about 0.1 V above the plasma potential and its negative end around 0.9 V below plasma potential (ref. 14). This large negative field region attracts the thermal ions from the thruster, and their rate of collection limits the return current to the vehicle.

Return Current Theory

The range of spacecraft generated electric fields determines the volume of plasma that can supply return current. The electric field around a naturally charged spacecraft extends outward only a few Debye lengths (see table II) because of shielding by the ambient plasma. For high voltage solar arrays, however, the shielding length is larger, and it is necessary to determine the scaling with array voltage.

When the applied potential energy eV is much greater than the thermal kinetic energy kT, the ions are pulled from the plasma with nearly zero energy (kT), and the electron space charge becomes exponentially small just a few Debye lengths from the plasma edge. Under these conditions the Langmuir-Childs space-charge analysis applies (refs. 15, 16). The ion current density flowing from the background plasma to a negative satellite surface is

$$j_{L.C.} = \frac{(2e/M)^{1/2} V^{3/2}}{9\pi\beta^2 x^2} \tag{11}$$

where β^2 is a geometry factor and x is the distance between the source plasma and the collector. The ion current j_i collected by the surface is limited to that available from the surrounding environment, including the ambient plasma ions and ram current on forward surfaces (due to spacecraft motion), as well as ion thruster sources.

The separation x is determined by limiting $j_{L.C.}$ to the available j_i that can be drawn from the surrounding region. For the geosynchronous situation where $j_i = ne\bar{v}$, equation (11) has the solution

$$\beta x = \left[\frac{8\pi^{1/2}}{9}\right]^{1/2} \left[\frac{eV}{kT}\right]^{3/4} \left[\frac{kT}{4\pi ne^2}\right]^{1/2} \tag{12}$$

Note that βx is independent of particle mass, and thus applies to ion- or electron-collecting sheaths. The factor β is unity for plane-parallel geometry (or any curved surfaces with βx much less than a typical dimension) but may vary substantially for other geometries (ref. 16).

For the conditions of geostationary orbit, a plane electrode at 10 kV would have a shielding length of ∿7 km. Thermal plasma bubbles produced by ion thrusters on booms even one kilometer away would be within the range of the electric fields from the spacecraft.

Solar Power Satellite Applications

As an illustration of the space charge limit on return current, consider station keeping of the solar power satellite (SPS) at GEO. One version of the SPS system (ref. 6) has 25 control thrusters located on a 0.5 km boom extending from each corner of the solar array rectangle. Operating

characteristics are those of the 100 cm argon thruster listed in table I. The solar panel is designed to operate at 40 kV so that its central power mains are around 4 kV positive and 36 kV negative with respect to the external plasma. At the edge of the array near the boom the panel potential is midway between the mains.

Consider first the case where the coaxial power line to the thrusters is unshielded with its exterior surface at the negative potential. The thermal ions are attracted to the cable by its external fields. The amount of current that this cable can collect has been estimated using the methods developed by Langmuir (refs. 15, 16) and treating the cable as a rectangular strip of length L and width πa. The running integral of the charge limited current starting from the end of strip away from the source and stopping at the thruster cluster radius r_o is given by the expression

$$I(>z) = \frac{4\pi\epsilon_o a}{L}\left(\frac{2e}{M}\right)^{1/2} V^{3/2}\left[\frac{\cos\theta}{(1-\cos\theta)} + \ell n\,(1-\cos\theta)\right] \qquad (13)$$

where $$\theta = \sin^{-1}(z/L) \qquad r_o \leq z \leq L \qquad (14)$$

The plot of $I(>z)$ in figure 6 demonstrates the concentration of current density near the thruster. The SPS thruster cluster at the end of the boom produces about 200 A of thermal plasma, and the integral $I(r_o)$ over the 500 m boom reveals that about 300 A could be collected on a 1 m coaxial cable.

This current collection can be eliminated by suitable insulation around the conducting surfaces. But the high voltage solar panels provide an alternate sink for thermal ions. The space-charge limited current capacity of such surfaces is described by equation (13) as well, and the current density has a profile similar to that in fig. 6. A schematic diagram of the current flow to SPS is shown in fig. 7. Most of the charge would be collected in the corner region where the boom attaches to the main structure. The enormous dimensions of the collecting surface imply that all of the thermal ion current would be collected by the exposed solar cell interconnects.

Insulating the entire solar panel surface would eliminate this return current path. However, this insulation membrane must be able to withstand high voltages that are created by charge collection on the outer surface. Laboratory experiments with plastic materials such as Kapton have been performed (ref. 17), and the material suffered breakdown and pinhole formation at the edges of conducting elements. Development of new materials or somewhat thicker membranes presumably will be needed to withstand the electric fields. Thus, to avoid solar panel breakdown, collection of thermal return currents on bare coaxial cable appears to be a more desirable procedure.

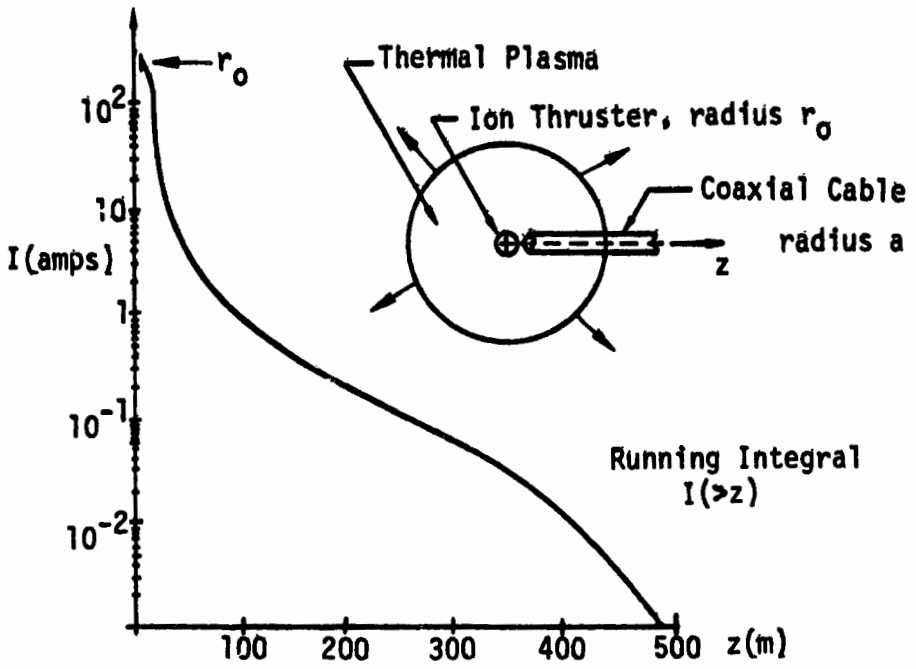

Figure 6. - Space-charge-limited current collected by exposed boom cable to thruster cluster on SPS.

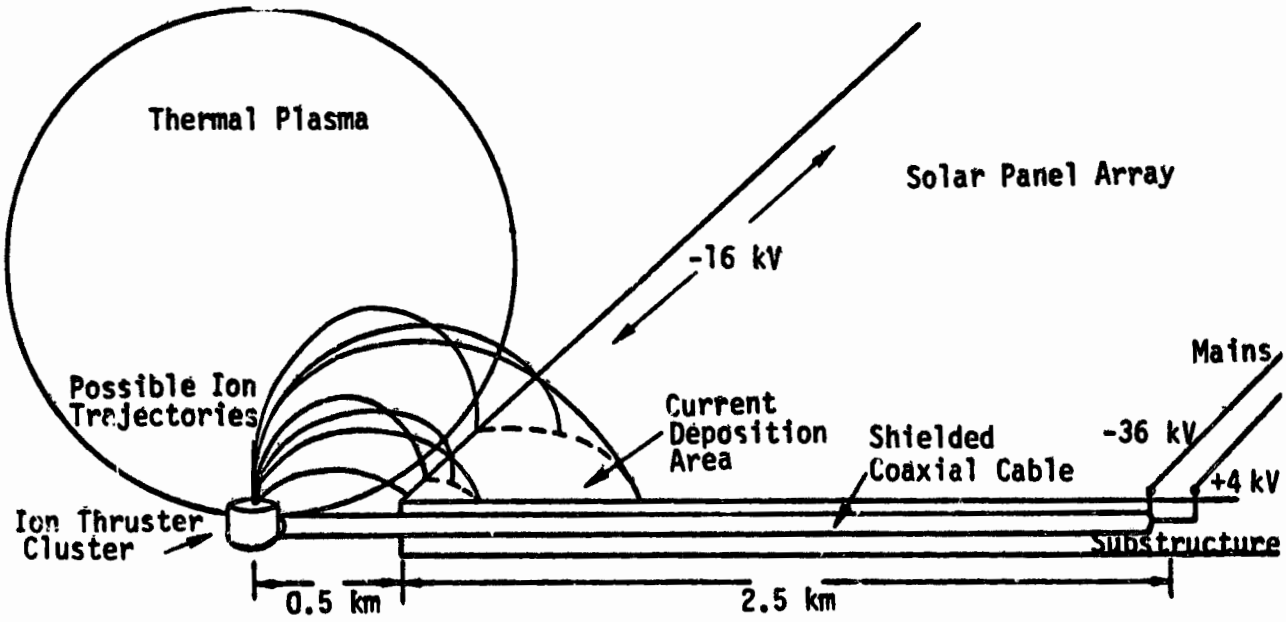

Figure 7. - Thermal ion current collected by unshielded solar cell interconnects on SPS panels.

APPENDIX. THERMAL ION GENERATION

Charge-Transfer Plasma

The slow neutrals are assumed to expand spherically as if they originated at a point a distance r_o behind the accelerating mesh. The fast ions are assumed to flow in a constant radius cylinder over the range where the neutral density is high enough to support charge transfer. Because a significant fraction of the original ion beam undergoes charge transfer, it is necessary to solve the coupled equations for the densities of fast and slow ions.

Momentum transfer during charge transfer collisions can be neglected. However, we also neglect the effects of momentum changing collisions, which is not entirely justified and would have a significant effect on the thermal plasma expansion. In the expansion calculations, we have used spherical expansion rather than cylindrical expansion (as implied by the potential model) as a crude way of accounting for the typical forward motion of the thermal particles acquired in elastic collisions with beam particles.

Slow ion creation and loss:

$$\frac{dn_s^+}{dt} = \nabla \cdot j_s^+ = \frac{\sigma(v_f - v_s)}{v_f\, v_s} (j_f^+ j_s - j_s^+ j_f) \tag{1}$$

where

$$j_s^+ = n_s^+ v_s \text{ etc., and}$$

$$j_f = j_f^+ + j_f^o \; ; \; j_s = j_s^+ + j_s^o \, ,$$

and σ is the charge transfer cross-section.

Fast ion creation and loss:

$$\frac{dn_f^+}{dt} = -\nabla \cdot j_f^+ = \frac{\sigma(v_f - v_s)}{v_f\, v_s} (j_s^+ j_f - j_f^+ j_s) \tag{2}$$

$$-\frac{dn_f^+}{dt} = \frac{dn_s^+}{dt} \tag{3}$$

Taking Z = 0 at the effective center of spherical expansion for the slow particles, and letting

$$j_s = I_o/Z^2 \quad , \quad j_s^+ = I_o^+/Z^2 \tag{4}$$

we have

$$\nabla \cdot j_s = \frac{1}{Z^2} \frac{\partial}{\partial Z} (Z^2 j_s) \text{ when operating} \tag{5}$$

on j_s , j_s^+ , j_s^o , and

$$\nabla \cdot j_f = \frac{\partial}{\partial Z} j_f \tag{6}$$

Combining (4) and (5) and defining slow fluences $\bar{v}_s$, $\bar{v}_s^+$ by

$$j_s = \bar{v}_s/Z^2 \ , \ j_s^+ = \bar{v}_s^+ (Z)/Z^2 \tag{7}$$

we obtain a differential equation for the slow ion fluence,

$$\frac{\partial^2 j_s^+}{\partial Z^2} + \left(\frac{j_s}{KZ^2} + \frac{j_f}{K}\right) \frac{\partial j_s^+}{\partial Z} = 0 \tag{8}$$

where

$$K = \frac{v_f \, v_s}{\sigma(v_f - v_s)} \tag{9}$$

The solution of equation (8) is

$$\frac{\partial j_s^+}{\partial Z} = a \, e^{-p(Z)} \tag{10}$$

when

$$p(Z) = \frac{j_s}{K} \left(\frac{1}{Z_o} - \frac{1}{Z}\right) + \frac{j_f}{K} (Z - Z_o) \tag{11}$$

where Z_o is the thruster exit position, i.e., $Z_o \approx r_o$, the exit radius. Since $p(Z_o) = 0$, the constant a is given by the initial value of the charge transfer rate,

$$a = \frac{j_f \, j_s}{K \, Z_o^2} \tag{12}$$

Thus the slow ion source distribution is

$$\frac{\partial j_s^+}{\partial Z} = \frac{j_f \, j_s}{K \, Z_o^2} \, e^{-p(Z)} \tag{13}$$

and the net slow ion current is

$$j_s^+(Z) = \frac{j_f \, j_s}{KZ_o^2} \int_{Z_o}^{Z} e^{-p(Z)} \, dZ \tag{14}$$

Thermal Ion Acceleration

The thruster beam is emitted over an area A_o with average density n_b and speed v_b such that

$$I_b = e\, n_b\, v_b\, A_o \tag{1}$$

where

$$\frac{1}{2} M v_b^2 = eV_b - eV_n \tag{2}$$

where M is the ion mass, V_b is the beam accelerating voltage, and V_n is any ion retarding potential which builds up between the outer accelerating grid (vehicle skin) and the beam in order to pull in sufficient electrons from the neutralizer to balance the ion space charge.

The region near the vehicle skin where the drop V_n occurs is assumed to be small compared to the charge transfer mean free path, and we will also assume that relatively few slow charge transfer ions move backward to the grid (both of these approximations are substantiated by the results). Then the total positive charge density near the exit grid is $e\, n_b$. Overall space charge neutrality requires that

$$n_e = n_b \tag{3}$$

The electrons are supplied by a plasma source mounted on one side of the thruster. The open area of the plasma source is much smaller than A_o. The outer structure of the neutralizing plasma source is grounded to the outer structure of the thruster. This plasma can be assumed to have an electron temperature of $\gtrsim$1 eV and an ion temperature of perhaps 0.1 eV. Since the net current emitted by the vehicle must be zero, the neutral plasma must be the source of a current, I_e.

Drawing this current from the plasma to the beam requires the voltage V_n, i.e.,

$$I_e\,(V_n) = -I_b \tag{4}$$

The functional form for the neutralization current is the Langmuir-Childs equation (ref. 15):

$$I_e = A\, j_{L.C.} = \frac{(2e/m)^{1/2}\, V_n^{3/2}}{9\pi\beta^2 \ell^2} A_n \tag{5}$$

where m is the electron mass, ℓ is the separation between the beam and the thruster plasma, β is the appropriate geometrical factor, and A_n is the emitting area of the neutralizing plasma. Equations (4) and (5) determine V_n, the difference between the potential at the center of the beam and the vehicle skin potential,

$$V_n = \left\{ \frac{9}{\sqrt{\frac{2e}{m}}} \left[\frac{\pi(\beta\ell)^2}{A_n} \right] I_b \right\}^{2/3} \tag{6}$$

Evaluating the constants

$$V_n = 5.7 \times 10^3 \left[\frac{I_b(\beta\ell)^2}{A_n} \right]^{2/3} \quad \text{(Volts)} \tag{6a}$$

we se that $\beta\ell$ must be very small or A_n must be large in order to explain the observed drops of just a few tens of volts between the beam center and the surrounding space.

It is impossible to obtain a large emitting area, with the small emitter presently in use and the low ion temperatures characteristic of these plasma generators.

The gap, however, can be quite small. We shall see below that the charge transfer plasma density is approximately 2.6×10^{10} cm^{-3}. The space charge shielding length for these ions, assuming a temperature of 1000°K, is $\lambda_t \simeq 7(T_t/n_{th})^{1/2}$. The expression for the voltage required to emit I_b across a gap determined by a shielding plasma is

$$V_n = 7.7 \times 10^4 \left[\frac{I_b T_o}{A_n n_t} \right]^{1/2} \tag{7}$$

For a current of 80 amps and the above plasma characteristics, equation (7) gives

$$V_n = 15.4 \text{ volts}$$

Without the charge transfer plasma, V_n would be much larger.

REFERENCES

1. Worlock, R.; Trump, G.; Sellen, J. M., Jr.; and Kemp, R. F.: Title Unavailable. AIAA Paper 73-1101, 1973.

2. Bartlett, R. O.; DeForest, S. E.; and Goldstein, R.: Spacecraft Charging Control Demonstration at Geosynchronous Altitude. AIAA Paper 75-359, March 1975.

3. Komatsu, G. K.; Sellen, J. M., Jr.; and Zafran, S.: Ion Beam Plume and E-Flux Measurements of an 8 cm Mercury Ion Thruster. To be published in J. Spacecraft and Rockets.

4. Kaufman, H. R.; and Isaacson, G. C.: The Interactions of Solar Arrays with Electric Thrusters. AIAA Paper 76-105, 1976.

5. Austin, R. E.; Dod, R. E.; and Grim, D.: Solar Electric Propulsion for the Halley's Comet Rendezvous Mission: Foundation for Future Missions. AIAA Paper 78-83, Jan. 1978.

6. Solar Power Satellite System Definition Study Part III, Preferred Concept System Definition. G. R. Woodcock, Mr., Boeing Rpt. D180-24071-1, NAS-15196, DRL T-1346, DRD MA-664T, March 1978.

7. Staggs, J. F.; Gula, W. P., and Kerslake, W. R.: Distribution of Neutral Atoms and Charge-Exchange Ions Downstream of an Ion Thruster, J. Spacecraft 5, Feb. 1968, pp. 159-164.

8. Liemohn, H. B.: Electrical Charging of Shuttle Orbiter, IEEE Trans. Plasma Science, PS-4, Dec. 1976, pp. 229-240.

9. McPherson, D. A.; Cauffman, D. P.; and Schober, W. R.: Spacecraft Charging at High Altitudes: SCATHA Satellite Program. J. Spacecraft 12, Oct. 1975.

10. Rossi, B.; and Olbert, S.: Introduction to the Physics of Space, McGraw-Hill, 1970, pp. 157-187.

11. Liemohn, H. B.: Radiation Belt Particle Orbits, Boeing Rpt. D1-82-0116, June 1961.

12. Chen, F. F.: Electric Probes, in Plasma Diagnostic Techniques. Huddlestone, R. H.; and Leonard, S. L.; editors. Academic Press, 1965, pp. 113-200.

13. Swift, J. D.; and Schwar, M.J.R.: Electrical Probes for Plasma Diagnostics. American Elsevier, 1970, pp. 137-155.

14. Stevens, N. J.; Spacecraft-Charged-Particle Environment Interactions. (Paper 3-1) Proc. Spacecraft Charging Technology Conference, C. P. Pike and R. C. Finke, editors, 1979.

15. Langmuir, I.; and Blodgett, K.: Currents Limited by Space Charge Between Coaxial Cylinders. Phys. Rev. 21, 1923, pp. 347-356.

16. Cobine, J. D.: Gaseous Conductors: Theory and Applications. Dover Publications, New York, 1958, pp. 123-128.

17. Kennerud, K. L.: High Voltage Solar Array Experiments. Boeing Rpt. to NASA/LeRC, GR 12180, Mar. 1974.